

1
2
3

Study of (p,n) reaction in a wide energy range

Abstract

5

6 In this paper, the quasi-elastic scattering (p, n) reactions are studied for a wide range of target nuclei ^{13}C , ^{14}C , ^{48}Ca , ^{90}Zr and ^{208}Pb and different incident energies (35-160 MeV). The phenomenological Optical model potential and density independent approaches are used for these calculations in comparison with density dependent semi-microscopic approach. The density dependent parameters are modified to achieve the best calculations for many targets at different energy levels.

12

Keywords: quasi-elastic scattering, single folding, lane potential.

14

PACS 24.50.+g,25.60.Bx,25.60.Lg,

16

17

18

1. Introduction

20

21 Examinations of the elastic and quasi-elastic scattering of neutrons and protons is one simple way for better understanding the character of the nuclear interaction. The isospin is one important and interesting feature of the nucleon-nucleus interactions. In order to be determined, Lan24[1] postulated a straightforward reliance of the nucleon-nucleus optical potential upon the isospin operators in terms of the optical model (OM). The matrix elements ensuing from this dependence are expressed in simple forms [2] for both of the (p,p), (n,n), and the (p,n) reactions.

27

28 Also, more realistic method is using the folded nucleon-nucleon (NN) interaction potential in the framework of OM. The folded potential represents the real part of the optical potential [3-5]. With this method, antisymmetrization of the investigated system has been mulled over to incorporate the exchange terms [6].

32

33 We represent here a systematic study of the (p,n) reactions in the framework of the OM, in which the interaction potential is engendered by folding the chosen potential with the densities of the nucleus. The NN interactions are taken in the form of sums of direct and zero range exchange terms. Supplementally, phenomenological OM is used to describe the same reactions. It is an extension to our previous work [7].

38

2. The Lane Model

40

41 The nuclear interaction between an incident nucleon and a target with non-zero isospin has an isospin dependent part. The lane isospin dependent part is formulated as

43

44

$$\frac{4\pi T}{A} U_1 , \quad (1)$$

where, U_1 is known as the Lane potential that contributes to both the elastic (p,p) and (n,n) scattering just as to the charge exchange (p,n) reaction. The isospin of the particle and target nucleus, are t, T , respectively and A is the mass number of the target. Thus, in a straightforward method, lane potential (isospin dependent part) is connected to optical potential to form the total nuclear nucleon-nucleus interaction as

$$50 \quad U = U_o + \frac{4tT}{A} U_1. \quad (2)$$

51 Knowledge of U_1 is of key enthusiasm for investigations of nuclear phenomena in which neutrons and protons are different (isovector modes). Numerous past appraisals of U_1 are liable to serious uncertainties as Distorted Wave Born Approximation (DWBA) analysis of (p,n) reactions. For instance, in the comparison of elastic nucleon scattering from different nuclei one must make assumptions [2] about the variation of nuclear geometry with A and ε . It is on a fundamental level conceivable to stay away from these uncertainties by extracting U_1 from a consistent study of the elastic proton and neutron scattering and the charge exchange (p,n) reaction on the same target nucleus, at the same energy. We recall here briefly the consistent isospin coupling scheme [1] for the elastic nucleon-nucleus scattering and charge exchange (p,n) reaction exciting.

60

61 The matrix elements resulting from equation (2) give the following relationships [2].

$$62 \quad U_{pp} = U_o - \frac{N - Z}{A} U_1 \quad (3)$$

$$63 \quad U_{nn} = U_o + \frac{N - Z}{A} U_1 \quad (4)$$

64 Similarly, the transition matrix element or (p,n) form factor for the charge exchange reaction is

$$66 \quad U_{pn} = \frac{2(N - Z)^{1/2}}{A} U_1 \quad (5)$$

Accordingly

$$68 \quad U_{nn} - U_{pp} = \frac{2(N - Z)}{A} U_1 = (N - Z)^{1/2} U_{pn} \quad (6)$$

where $\varepsilon = \frac{N - Z}{A}$

70 The present calculations of angular distributions of the (p,n) elastic scattering cross sections were made by using the distorted-wave code DWUCK4 [8], and the optical potential is

$$72 \quad U_{pp(nn)}(R) = N_R \left[V_{F0}(R) \pm \frac{N - Z}{A} V_{F1}(R) \right] + iW(R), \quad (7)$$

for (n,n), (p,p), and for (p,n) reaction

$$74 \quad U_{pn}(R) = \frac{2(N - Z)^{1/2}}{A} [N_R V_{F1}(R) + iW(R)], \quad (8)$$

where $V_{F0(1)}(R)$ is the nuclear real potential calculated by the folding procedure, including the zero range exchange part of the potential by using DFPOOT code [9]. $W(R)$ is the imaginary part of the potential including both type; volume $W_V(R)$ and surface $W_S(R)$.

78 The last outcomes for the angular distributions of scattering cross sections were gotten by
 changing the parameters of the imaginary part of the potential to get the best fit with the
 experimental values.

81

3. Method of Calculations

83

84 In this work, we study the quasi-elastic scattering (p,n) reaction. Differential scattering cross
 sections are determined for a wide range of incident proton energies by different targets. Initially,
 proton of energies 35, 45 and 135 MeV [10,111] incident on target nuclei ^{48}Ca . Pursued by, proton of
 energies 35, 45, 120 and 160 MeV [10,13,14] incidents on target nuclei ^{90}Zr . Then, proton of
 energies 35 and 45 MeV [9] incidents on target nucleus ^{208}Pb . At long last, proton of energies 35
 and 45 MeV [15,16] incidents on target isotope nuclei ^{13}C and ^{14}C , respectively.

90

3.1 The phenomenological Optical potential

92

93 The global WS parameters for different nucleon potentials [17-19] have been carefully
 determined based on large experimental data bases of the elastic nucleon-nucleus scattering. Then,
 it has been found to be useful in calculation of the transition optical potential (Upn).

94 We have been chosen CH89 global optical parameters as initial parameters, and in that case
 a minor change is needed to reproduce the best fit of the scattering cross sections with the
 experimental data in the optical model (OM) analysis. The equations and parameters used in
 potential CH89 are listed in ref.[18].

100

3.2. Density independence folding potential

102

103 The nucleon-nucleus potential can be obtained by single folding (SF) the density distribution
 of the target nucleus $\rho_T(r)$ with the NN effective interaction $V_{NN}(S)$ [20]

105

106

$$V_F(R) = \int \rho_T(r) V_{NN}(S) dr , \quad (9)$$

where $S = |R - r|$ is the distance between the two nucleons. Here, we take the NN interaction to be
 density independent (DI) M3Y effective NN interaction with a zero-range approximation in the
 form

$$(10) (V_{NN})_o(s) = 7999 \frac{e^{-4s}}{4s} - 2134 \frac{e^{-2.5s}}{2.5s} - 276 [1 - \alpha\varepsilon] \delta(s) \quad 110$$

$$\text{and} \quad (V_{NN})_1(s) = -4886 \frac{e^{-4s}}{4s} + 1176 \frac{e^{-2.5s}}{2.5s} + 228 [1 - \alpha\varepsilon] \delta(s) . \quad 111$$

112

V_0 and V_I are the (isoscalar and isovector) M3Y effective NN interaction potential respectively,
 supplemented by zero range potentials. Where (α) is the energy dependent parameter = 0.005
 MeV. The zero range potential (third term) in equations (10) and (11) represents the single nucleon
 exchange term.

117

118 Consequently, the real folded isoscalar $V_{F0}(R)$ and isovector $V_{FI}(R)$ components of $V_F(R)$
 potentials are calculated and further scaled by a factor N_R in addition to $W(R)$ to obtain $U_{0(1)}$.

120

3.3. Density dependence folding potential

122

123 The failure of simple M3Y-NN type interactions to give a good description of the data in
 many cases [21-24], leads to the inclusion of explicit density dependence. In consequence, the
 other type (DD) of the SF potential is introduced as follow

126

127

$$V_F(R) = g(\rho, \varepsilon) \int \rho_T(r) V_{NN}(S) dr . \quad (12)$$

The density dependence [25] adopted is

129

$$g(\rho, \varepsilon) = C(1 - \beta(\varepsilon) \rho^n) . \quad (13)$$

The density dependent parameters C and β , can be given by the subsequent

131

132

$$\beta = [(1 - P)\rho_0^{-n}][(3n + 1) - (n + 1)P]^{-1} , \quad (14)$$

133

134

$$P = (10 m \varepsilon_0) (\hbar^2 k_0^2)^{-1} , \quad (15)$$

135

136

$$c = -(2 \hbar^2 k_0^2) [5mJ_0 \rho_0 (1 - (n + 1)\rho_0^n \beta)]^{-1} . \quad (16)$$

137

138 It is quite obvious that density dependence parameter (β) obtained by this method depends only on the saturation energy per nucleon (ε_0), the saturation density (ρ_0) and the index (n) but not on the parameters of the M3Y interaction while the parameter (c) depends on and also through the volume integral (J_0).

142

143 As a result, the two parameters β and C are chosen to have different values with different investigated energies. Thus, the density dependent factor $g(\rho, \varepsilon)$ is turn out to be function of energy. The value of parameter $n = 2/3$ was firstly taken by Myers in the SF calculation [25]. Three forms are applied in our analysis which is summarized according to energy range used as:

147

148

$$g(\rho, \varepsilon) = 2.07(1 - 1.667 \rho^{2/3}) \quad (17)$$

149 this denoted as DD1 within energy range 120-160 MeV, where $\rho_0 = 0.15$ [26,27],

150

151

$$g(\rho, \varepsilon) = 2.85(1 - 1.614 \rho^{2/3}) \quad (18)$$

152 this indicated as DD2 at energy 45 MeV, where $\rho_0 = 0.16$ [28,29], and

153

154

$$g(\rho, \varepsilon) = 1.55(1 - 1.054 \rho^{2/3}) , \quad (19)$$

155 this referred to as DD3 at energy 35 MeV, where $\rho_0 = 0.28$ [30,31].

156 Notice that, $g(\rho, \varepsilon)$ in equation (13) is a function of energy at only one value at saturation. The 157 was our trial to be obtained as a variable function with changing energy. According to the 158 investigated results, it is appropriate to improve the value of ρ_0 to be as a function in energy to 159 generate and achieve the three ranges. This is represented by:

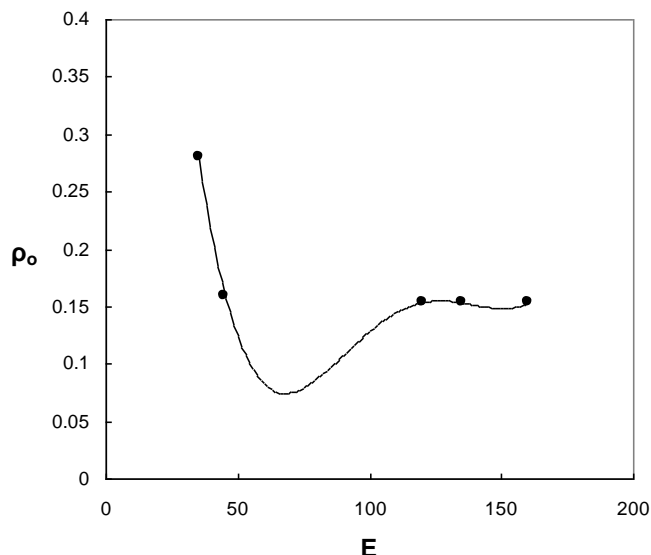
160

161 $\rho_0 = 10^{-8} E^4 - 5 \times 10^{-6} E^3 + 8 \times 10^{-4} E^2 - 0.058 E + 1.47$. (20)

162

163 Consistent with the above formula, it is proper to draw the relation that shows the variation of ρ_0
164 with E in the figure (1) as following:

165



166

167

168 Fig.(1): the variation of different values of saturation density (ρ_0)
169 with different energies (E)

170

171 Summarizing that, we are used the SF program to calculate the real parts of the
172 nucleus-nucleus scattering of several systems. The interactions are divided into density
173 independence M3Y-DI and density dependence DD1, DD2 and DD3 interaction. From the
174 description, the basic inputs to a folding calculation are nuclear densities of the target
175 nucleus and the effective NN interaction. The densities of ^{13}C and ^{14}C are taken as Gaussian [32],
 ^{48}Ca [33], ^{90}Zr [34] and ^{208}Pb [35] are taken as Fermi. In the present work, we examine a few
176 representative cases about the real part of nuclear potential. These data are very helpful to test
177 the modified density dependent Folding potential.

178

4. Results and Conclusion

181

182 In this work, the phenomenological OM and semi-microscopic (SF) model are used. The
183 DI and DD1, DD2 and DD3 effective NN interaction is employed to drive the real folding optical
184 model potentials of the investigated systems, assuming the density distribution for different targets
185 nuclei. The imaginary potentials are supplemented to the derived potentials in phenomenological
186 Woods-Saxon (WS) form. The quasi-elastic angular distributions for the different systems are
187 calculated and the results are compared to the experimental data.

188

189 The Figures (2-12) show the cross section data for the quasi elastic scattering using different
190 potentials for the investigated nuclei at low and high energies. It is easy to notice from these
191 figures that, all the used potentials give a good results for the scattering cross sections of each of
192 the reactions (p,n), although these potentials have different characteristic values. This is due to the

fact¹⁹³ that the calculations of the interaction cross sections depend also up on the imaginary potential.

195

¹⁹⁶ harmony with the success of density and energy dependent in the analysis of quasi-elastic scattering¹⁹⁷ (p,n) reaction, it is interested to study how far the calculated Unn and Upp are consistent with¹⁹⁸ pn in equation (5). So, the calculations were done to get Unn and Upp by changing the potential¹⁹⁹ according to equations (3) and (4). The Unn, Upp and Upn characteristics of the investigated nuclei for the used potentials are presented in Tables (1-11).

200

²⁰¹ Generally, we concluded that using the modified density dependent single folding model successfully²⁰² describes the quasi-elastic scattering experimental data at different energy ranges and gives²⁰³ good agreement of the calculated values of Unn and Upp with equation (5).

204

205

206

207

208

209

References

211

- [1] ²¹²M. Lane. Nucl.Phys. 35, 676 (1962).
- [2] ²¹³D Carlson, C.D. Zafiratos Nucl. Phys. A., 249, 29 (1975).
- [3] ²¹⁴R. Satchler, K.W. Mcvoy, Nucl. Phys. A, 522: 621 (1991).
- [4] ²¹⁵B. Arellano, Phys. Rev. C 66:24602(2002).
- [5] ²¹⁶A.Ogloblin, Yu.Aglukhov, Phys. Rev. C 62: 44601 (2000).
- [6] ²¹⁷T.Khoa, G.R.Satchler Nucl. Phys.A 668:3 (2000).
- [7] ²¹⁸A. El-Nohy, H. A. Motaweh, A. Attia , M. N. El-Hammamy, 20th International Seminar on Interaction of Neutrons with Nuclei: Alushta, Ukraine, 21–26 May (2012).
- [8] ²¹⁹D.Kunz, Abstract number NESC9872, 36 (1987).
- [9] ²²⁰Cook, Comput. Phys. Comm. 25,125 (1982).
- [10] ²²¹R.R. Doering, D.M. Patterson,A. Galonsky, Phys. Rev. C 12, 378 (1975). 222
- [11] ²²²E. Bainum, J. Rapaport, C. D. Goodman et al., Phys. Rev. Lett. 44, 1751 (1980). 223
- [12] ²²³E. Sugarbaker et al., Proceedings of the International Conference on Nuclear Structure, Amsterdam, 1982, edited by A. Van Der Wonde and B. J. Verhaar, pp. 77. 224
- Jacob Rapaport (private communication) 225
- [13] ²²⁴Orihara, T. Murakami, Nucl. Instrum. Methods 181, 15 (1981). 226
- [14] ²²⁵Orihara et al., Nucl. Instrum. Methods Phys. Res. A257, 189 (1987).
- [15] ²²⁶Jacob Rapaport, unpublished (private communication).
- [16] ²²⁷D.Anderson, M.Mostajabodda'vati, C.Lebo et al., Phys.Rev.C43,1630 (1991).

- [17] D. Becheetti, G.W. Greenlees, Phys. Rev. 182, 1190 (1969).
- [18] L. Varner, W.J. Thompson, T.L. McAbee, E.J. Ludwig, T.B. Clegg, Phys. Rep. 201, 57 (1991).
- [19] A.J. Koning, J.P. Delaroche, Nucl. Phys. A713, 231 (2003)
- [20] R. Satchler, W.G. Love, Phys. Rep. 55, 183 (1979).
- [21] G. Bohlen, M.R. Clover, G. Ingold et al., Z. Phys. A 308, 121 (1982).
- [22] G. Bohlen, X.S. CHEN, J.G. Cramer et al., Z. Phys. A 322, 241 (1985).
- [23] Stiliaris, H.G. Bohlen, P. Frobrich et al., Phys. Lett. B223, 291 (1989).
- [24] N. Basu, P. Roy Chowdhury, C. Samanta, Acta Physica Polonia B 37 (10), 2869 (2006).
- [25] D. Myers, Nucl. Phys. A204, 465 (1973).
- [26] Bandyopadhyay, C. Samanta, S.K. Samaddar, J.N. De, Nucl. Phys. A511, 1 (1990).
- [27] Roy Chowdhury, C. Samanta, D.N. Basu, Mod. Phys. Letts. A21, 1605 (2005).
- [28] Audi, A.H. Wapstra, C. Thibault, Nucl. Phys. A729, 337 (2003).
- [29] Satpathy, V.S. Uma Maheswari, R.C. Nayak, Phys. Rep. 319, 85 (1999).
- [30] Schutz et. al., Nucl. Phys. A599, 97c (1996).
- [31] Friedman, V.R. Pandharipande, Nucl. Phys. A361, 502 (1981).
- [32] Ozawa et al., Nucl. Phys. A 691, 599 (2001).
- [33] De Veries, and C.W. De Jager, Nucl. Data Tables 36, (1987) 495.
- [34] El-Azab Farid, M.A. Hassanain, Nucl. Phys. A678, 39 (2000).
- [35] Umemoto, S. Hirenzaki, K. Kume, H. Toki, Phys. Rev. C62, 024606 (2000).

250

251

252

253

254

255

256

257

258

259

260

261

262

Table 31: The best-fit parameters to (p,n) data of ^{90}Zr at 35 MeV within different models

Model	Channel	V MeV	r fm	a fm	W_v MeV	R_v fm	a_v fm	W_s MeV	R_s Fm	a_s fm
OM	(p,p)	70.97	1.062	0.8563	0.966	1.47	0.69	6.785	1.27	0.69
	(n ,n)	14.21	1.052	0.8454	0.696	1.27	0.69	5.878	1.27	0.69
	(p,n)	1.73	1.045	0.8795	1.326	1.16	0.69	0.00	0.00	0.00
DI	(p,p)	66.97	1.0427	0.8263	0.166	1.37	0.69	6.785	1.27	0.69
	(n ,n)	12.21	1.0427	0.8254	0.096	1.27	0.69	5.878	1.27	0.69
	(p,n)	1.830	1.0356	0.8595	1.366	1.17	0.69	0.00	0.00	0.00
DD1	(p,p)	71.97	1.0429	0.8263	0.866	1.47	0.69	6.785	1.27	0.69
	(n ,n)	14.21	1.0427	0.8254	0.596	1.27	0.69	5.878	1.27	0.69
	(p,n)	1.930	1.0360	0.8622	1.356	1.17	0.99	0.00	0.00	0.00
DD3	(p,p)	75.00	1.0427	0.8294	0.966	1.37	0.69	6.785	1.27	0.69
	(n ,n)	15.81	1.0431	0.8256	0.956	1.37	0.69	5.878	1.27	0.69
	(p,n)	1.930	1.0358	0.8611	1.206	1.17	0.69	0.00	0.00	0.00

264

265

266

267

268

269

270

271

272

273

274

Table 2: The best-fit parameters to (p,n) data of ^{90}Zr at 45 MeV within different models

Model	Channel	V MeV	r fm	a fm	W_v MeV	R_v fm	a_v fm	W_s MeV	R_s Fm	a_s fm
OM	(p,p)	68.72	1.049	0.8431	3.052	1.27	0.69	5.974	1.27	0.69
	(n ,n)	23.62	1.050	0.8380	3.080	1.27	0.69	5.098	1.27	0.69
	(p,n)	1.277	1.038	0.8875	1.152	1.29	0.69	0.00	0.00	0.00
DI	(p,p)	69.72	1.0391	0.8431	3.052	1.27	0.69	5.974	1.27	0.69
	(n ,n)	22.62	1.0402	0.8380	3.080	1.27	0.69	5.098	1.27	0.69
	(p,n)	1.177	1.0289	0.8875	1.152	1.29	0.69	0.00	0.00	0.00
DD1	(p,p)	75.72	1.0425	0.8467	6.052	1.27	0.69	5.974	1.27	0.69
	(n ,n)	25.62	1.0431	0.8421	4.080	1.27	0.69	5.098	1.27	0.69
	(p,n)	1.557	1.0324	0.8932	1.552	1.27	0.69	0.00	0.00	0.00
DD2	(p,p)	73.72	1.042	0.8466	6.052	1.27	0.99	5.97	1.27	0.69
	(n ,n)	24.62	1.0431	0.8412	4.080	1.27	0.99	5.09	1.27	0.69
	(p,n)	1.677	1.0322	0.8928	1.502	1.28	0.69	0.00	0.00	0.00

287
288
289

Table 3: The best-fit parameters to (p,n) data of ^{90}Zr at 120 MeV within different models

291

Model	Channel	V MeV	r fm	a fm	W_v MeV	R_v fm	a_v fm	W_s MeV	R_s Fm	a_s fm
OM	(p,p)	52.56	0.9663	1.057	7.73	1.27	0.69	1.338	1.27	0.69
	(n ,n)	31.84	1.203	0.9018	7.76	1.27	0.69	1.123	1.27	0.69
	(p,n)	1.905	0.885	1.277	0.38	1.27	0.69	0.00	0.00	0.00
DI	(p,p)	50.16	0.9963	1.007	7.730	1.27	0.69	1.388	1.27	0.69
	(n ,n)	30.59	1.0039	0.9818	7.760	1.27	0.69	1.123	1.27	0.69
	(p,n)	1.885	0.8557	1.377	0.430	1.27	0.69	0.00	0.00	0.00
DD1	(p,p)	50.16	0.9514	1.166	7.730	1.27	0.69	1.388	1.27	0.69
	(n ,n)	30.59	0.9584	1.146	7.760	1.57	0.69	1.123	1.27	0.69
	(p,n)	1.985	0.8588	1.394	0.350	1.27	0.69	0.00	0.00	0.00

292
293
294
295
296
297
298
299
300
301

302
303
304
305

Table 4: The best-fit parameters to (p,n) data of ^{90}Zr at 160 MeV within different models

307

Model	Channel	V MeV	r fm	a fm	W _v MeV	R _v fm	a _v fm	W _s MeV	R _s Fm	a _s fm
OM	(p,p)	60.50	0.951	1.273	5.794	1.27	0.99	0.509	1.27	0.69
	(n ,n)	38.81	0.951	1.158	8.196	2.27	0.59	0.406	1.27	0.69
	(p,n)	0.456	0.965	2.646	1.124	1.17	0.99	0.00	0.00	0.00
DI	(p,p)	61.90	0.9414	1.173	5.794	1.27	0.99	0.509	1.27	0.69
	(n ,n)	35.41	0.961	1.118	8.196	2.27	0.59	0.406	1.27	0.69
	(p,n)	0.356	0.955	2.546	1.124	1.17	0.89	0.00	0.00	0.00
DD1	(p,p)	55.90	0.9476	1.198	8.794	0.17	0.99	0.509	1.27	0.69
	(n ,n)	35.41	0.9673	1.140	8.196	0.37	0.69	0.406	1.27	0.69
	(p,n)	0.146	2.249	2.805	0.694	1.10	0.99	0.00	0.00	0.00

308
309
310
311
312
313
314
315
316

317

318

319

320

321

Table 5: The best-fit parameters to (p,n) data of ^{13}C at 35 MeV within different models

323

Model	Channel	V MeV	r fm	a fm	W_v MeV	R_v fm	a_v fm	W_s MeV	R_s Fm	a_s fm
OM	(p,p)	65.58	0.694	0.631	1.238	1.25	0.49	4.490	1.15	0.69
	(n ,n)	55.82	0.692	0.630	1.600	1.25	0.69	5.769	1.65	0.69
	(p,n)	0.784	0.635	0.658	2.700	1.43	1.10	0.00	0.00	0.00
DI	(p,p)	50.58	0.7944	0.7314	1.238	1.25	0.49	4.490	1.15	0.69
	(n ,n)	45.82	0.7927	0.7300	1.600	1.25	0.69	5.769	1.65	0.69
	(p,n)	0.584	0.8254	0.7389	2.700	1.44	0.95	0.00	0.00	0.00
DD1	(p,p)	48.98	0.8084	0.7315	1.638	0.55	0.69	4.49	1.15	0.69
	(n ,n)	45.02	0.8059	0.7309	1.600	2.55	0.69	5.76	1.15	0.69
	(p,n)	0.784	0.8505	0.7359	5.638	1.05	0.89	0.00	0.00	0.00
DD3	(p,p)	42.98	0.9530	0.7434	1.638	1.55	0.69	4.49	1.15	0.69
	(n ,n)	40.02	0.9488	0.7439	1.600	1.55	0.69	5.76	1.15	0.69
	(p,n)	0.284	1.0058	0.7393	6.638	0.98	0.89	0.00	0.00	0.00

324

325

326

327

328

329
330
331
332
333
334

Table 6: The best-fit parameters to (p,n) data of ^{14}C at 120 MeV within different models

336

Model	Channel	V MeV	r fm	a fm	W_v MeV	R_v fm	a_v fm	W_s MeV	R_s Fm	a_s fm
OM	(p,p)	39.50	1.255	0.650	8.756	1.25	0.69	1.239	1.15	0.69
	(n ,n)	22.50	1.177	0.669	5.761	1.25	0.69	0.936	1.15	0.69
	(p,n)	0.097	1.840	0.256	3.856	0.87	0.79	0.00	0.00	0.00
DI	(p,p)	35.50	1.1559	0.6001	8.756	1.25	0.69	1.239	1.15	0.69
	(n ,n)	20.50	1.0776	0.6494	5.761	1.25	0.69	0.936	1.15	0.69
	(p,n)	0.067	1.8409	0.2167	3.856	0.87	0.79	0.00	0.00	0.00
DD1	(p,p)	29.50	1.1551	0.6013	8.756	1.25	0.69	1.239	1.15	0.69
	(n ,n)	30.50	1.0775	0.6481	5.761	1.25	0.69	0.936	1.55	0.69
	(p,n)	0.097	1.8413	0.2216	3.856	0.87	0.79	0.00	0.00	0.00

337
338
339
340
341
342
343

344
345
346
347
348
349
350

Table 7: The best-fit parameters to (p,n) data of ^{48}Ca at 35 MeV within different models

352

Model	Channel	V MeV	r fm	a fm	W_v MeV	R_v fm	a_v fm	W_s MeV	R_s Fm	a_s fm
OM	(p,p)	36.16	1.158	0.69	3.27	1.11	0.69	7.073	1.11	0.69
	(n ,n)	32.79	1.158	0.69	3.90	1.11	0.69	3.420	1.11	0.69
	(p,n)	1.100	1.158	0.69	3.42	1.21	0.69	0.00	0.00	0.00
DI	(p,p)	70.27	0.9870	0.8826	2.270	1.21	0.69	7.073	1.11	0.69
	(n ,n)	35.85	0.9881	0.8782	2.900	1.21	0.69	3.420	1.11	0.69
	(p,n)	2.230	0.9779	0.9128	2.270	1.21	0.60	0.00	0.00	0.00
DD1	(p,p)	60.12	0.9966	0.8986	6.110	1.11	0.69	8.073	1.11	0.69
	(n ,n)	51.29	0.9977	0.8934	8.900	1.11	0.69	7.420	1.11	0.69
	(p,n)	0.882	0.9875	0.9304	4.100	1.21	0.55	0.00	0.00	0.00
DD3	(p,p)	62.12	0.9911	0.8905	4.510	1.11	0.69	0.173	1.11	0.69
	(n ,n)	45.29	0.9927	0.8849	8.110	1.11	0.69	5.42	1.11	0.69
	(p,n)	0.982	0.9820	0.9215	2.900	1.25	0.59	0.00	0.00	0.00

353

354

355

356
357
358
359
360
361
362
363

Table 8: The best-fit parameters to (p,n) data of ^{48}Ca at 45 MeV within different models

365

Model	Channel	V MeV	r fm	a fm	W _v MeV	R _v fm	a _v fm	W _s MeV	R _s Fm	a _s fm
OM	(p,p)	56.46	0.964	0.7512	1.184	1.21	0.69	6.163	1.11	0.69
	(n ,n)	41.81	0.924	0.9207	1.18	1.21	0.69	5.383	1.11	0.69
	(p,n)	0.145	1.054	0.1445	2.88	1.25	0.69	0.00	0.00	0.00
DI	(p,p)	60.46	0.9647	0.7812	1.184	1.21	0.69	6.163	1.11	0.69
	(n ,n)	40.81	0.9248	0.9107	1.180	1.21	0.69	5.383	1.11	0.69
	(p,n)	0.245	1.0549	0.1345	2.880	1.10	0.69	0.00	0.00	0.00
DD1	(p,p)	62.16	0.9724	0.7934	1.770	1.21	0.69	6.163	1.11	0.69
	(n ,n)	39.79	0.9319	0.9309	1.280	1.21	0.69	5.420	1.11	0.69
	(p,n)	0.200	1.0566	0.1329	2.520	1.21	0.69	0.00	0.00	0.00
DD2	(p,p)	48.16	1.040	06966	0.770	0.85	0.39	6.163	1.11	0.69
	(n ,n)	42.09	1.026	0.8091	2.780	1.21	0.69	5.42	1.11	0.69
	(p,n)	0.20	1.0563	0.1331	4.520	1.00	0.89	0.00	0.00	0.00

366

367

368
369
370
371
372
373
374
375
376

Table 9: The best-fit parameters to (p,n) data of ^{48}Ca at 135 MeV within different models

378

Model	Channel	V MeV	r fm	a fm	W_v MeV	R_v fm	a_v fm	W_s MeV	R_s Fm	a_s fm
OM	(p,p)	40.16	1.158	0.69	2.27	1.11	0.69	7.073	1.11	0.69
	(n ,n)	20.79	1.158	0.69	2.90	1.11	0.69	3.420	1.11	0.69
	(p,n)	0.100	1.158	0.69	1.22	1.11	0.79	0.00	0.00	0.00
DI	(p,p)	60.80	0.8755	1.041	2.77	1.11	1.19	0.950	1.11	0.69
	(n ,n)	30.10	0.8917	0.997	7.780	1.21	0.89	0.449	1.11	0.69
	(p,n)	0.10	0.4344	1.785	1.670	1.01	0.79	0.00	0.00	0.00
DD1	(p,p)	42.16	0.8818	1.071	1.270	1.11	0.69	7.073	1.11	0.69
	(n ,n)	24.09	0.8992	1.020	1.90	1.11	0.69	3.420	1.11	0.69
	(p,n)	1.300	0.3351	1.968	1.120	1.11	0.69	0.00	0.00	0.00

379

380

381

382

383
384
385
386
387
388

Table 10: The best-fit parameters to (p,n) data of ^{208}Pb at 35 MeV within different models

390

Model	Channel	V MeV	r fm	a fm	W_v MeV	R_v fm	a_v fm	W_s MeV	R_s Fm	a_s fm
OM	(p,p)	41.50	1.079	0.848	5.274	1.23	0.69	5.302	1.25	0.69
	(n ,n)	9.50	1.080	0.852	5.670	1.24	0.69	6.909	1.25	0.69
	(p,n)	1.552	1.076	0.854	2.474	1.04	0.57	0.00	0.00	0.00
DI	(p,p)	40.50	1.0896	0.8382	5.074	1.25	0.69	5.302	1.25	0.69
	(n ,n)	8.50	1.0902	0.8320	5.570	1.25	0.69	6.909	1.25	0.69
	(p,n)	1.352	1.0864	0.8644	2.574	1.01	0.55	0.00	0.00	0.00
DD1	(p,p)	38.50	1.0896	0.8398	3.074	1.75	0.89	5.302	1.25	0.69
	(n ,n)	14.50	1.0904	0.8333	3.570	1.55	0.89	6.909	1.25	0.69
	(p,n)	1.600	1.0864	0.8683	3.974	1.00	0.58	0.00	0.00	0.00
DD3	(p,p)	37.65	1.0887	0.8468	3.374	1.35	0.89	8.302	1.25	0.69
	(n ,n)	12.53	1.0936	0.7985	3.800	1.35	0.89	6.909	1.25	0.69
	(p,n)	0.250	1.0864	0.867	3.074	1.01	0.55	0.00	0.00	0.00

391

392

393

394

395

396

Table 11: The best-fit parameters to (p,n) data of ^{208}Pb at 45 MeV within different models

398

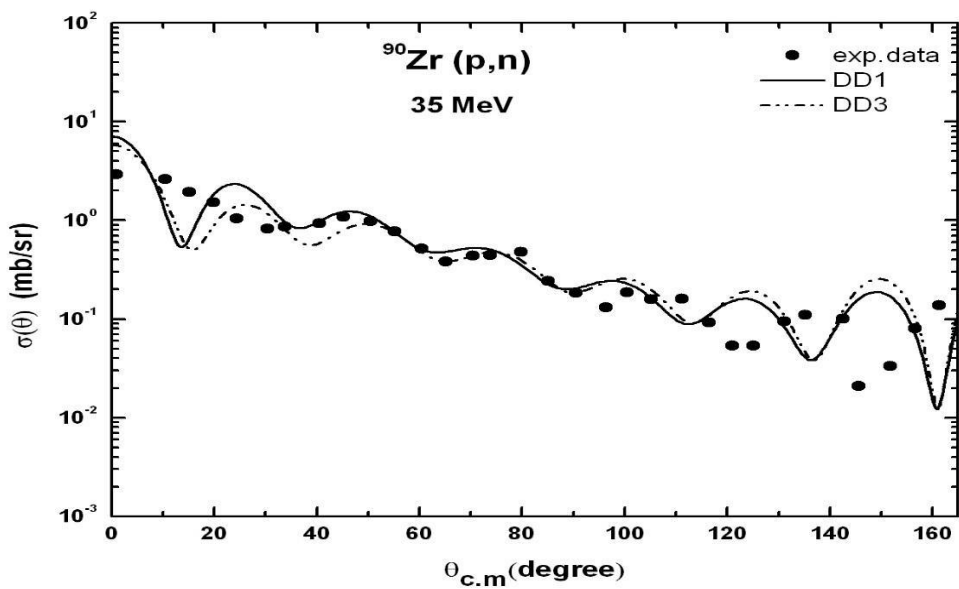
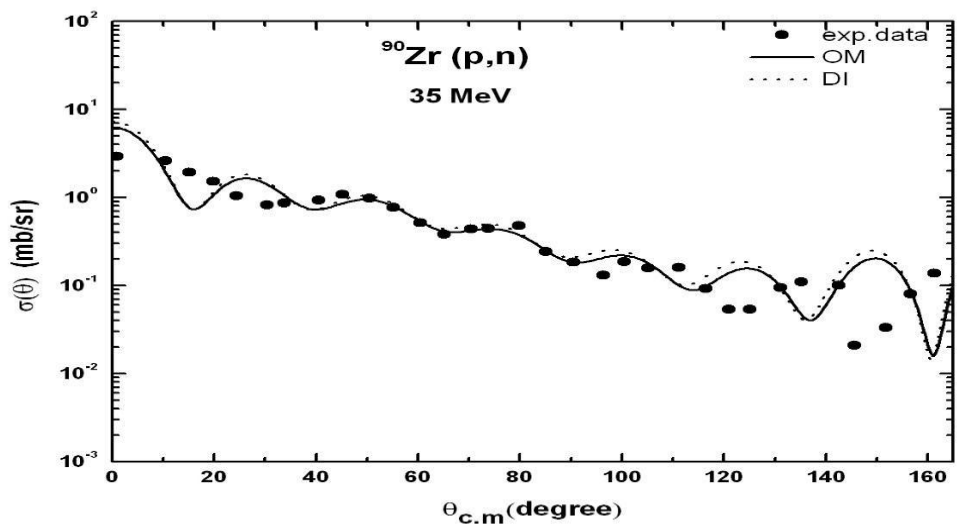
Model	Channel	V MeV	r fm	a fm	W_v MeV	R_v fm	a_v fm	W_s MeV	R_s Fm	a_s fm
OM	(p,p)	68.60	1.058	0.870	5.59	1.05	0.89	7.38	1.25	0.69
	(n ,n)	66.50	1.048	0.862	5.68	1.05	0.89	5.99	1.25	0.69
	(p,n)	2.35	1.053	0.858	2.29	1.19	0.79	0.00	0.00	0.00
DI	(p,p)	68.10	1.0881	0.8506	5.591	1.05	0.89	7.38	1.25	0.69
	(n ,n)	67.50	1.0889	0.8429	5.680	1.05	0.89	5.99	1.25	0.69
	(p,n)	2.55	1.0832	0.8881	2.291	1.20	0.79	0.00	0.00	0.00
DD1	(p,p)	70.61	1.0881	0.8523	5.791	1.01	0.85	7.38	1.25	0.69
	(n ,n)	65.03	1.0891	0.8455	5.980	1.01	0.85	6.03	1.25	0.69
	(p,n)	2.723	1.0833	0.8902	2.191	1.20	0.85	0.00	0.00	0.00
DD2	(p,p)	79.61	1.0882	0.852	3.791	1.20	0.65	7.388	1.25	0.69
	(n ,n)	36.03	1.0891	0.8458	0.980	1.20	0.65	6.030	1.25	0.69
	(p,n)	1.523	1.0833	0.890	0.911	1.31	0.75	0.00	0.00	0.00

399

400

401

402



403

Fig. (2): Quasi-elastic scattering for ^{90}Zr (p,n) at 35 MeV.

404

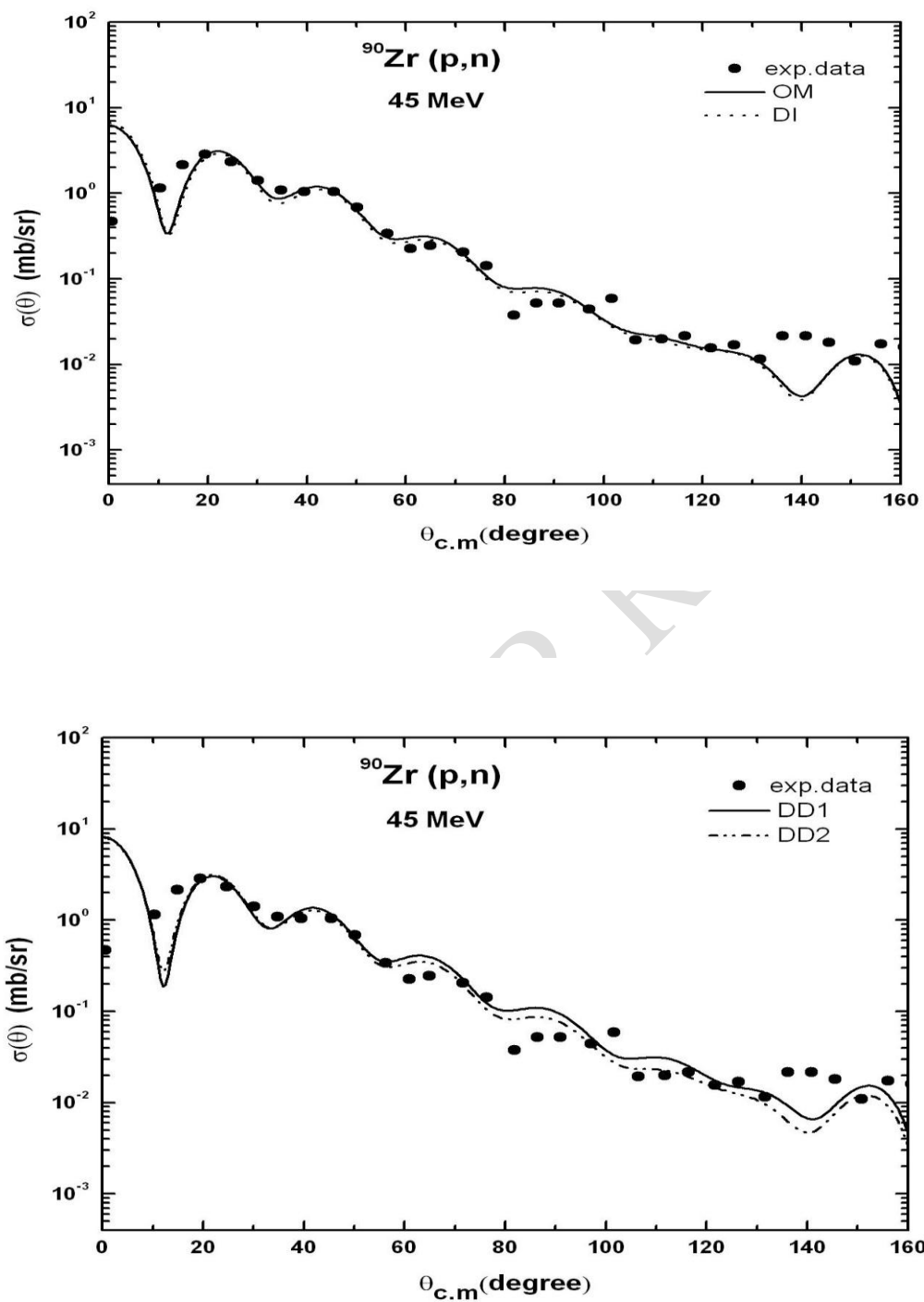
The data are taken from Ref.[10].

405

406

407

408



409

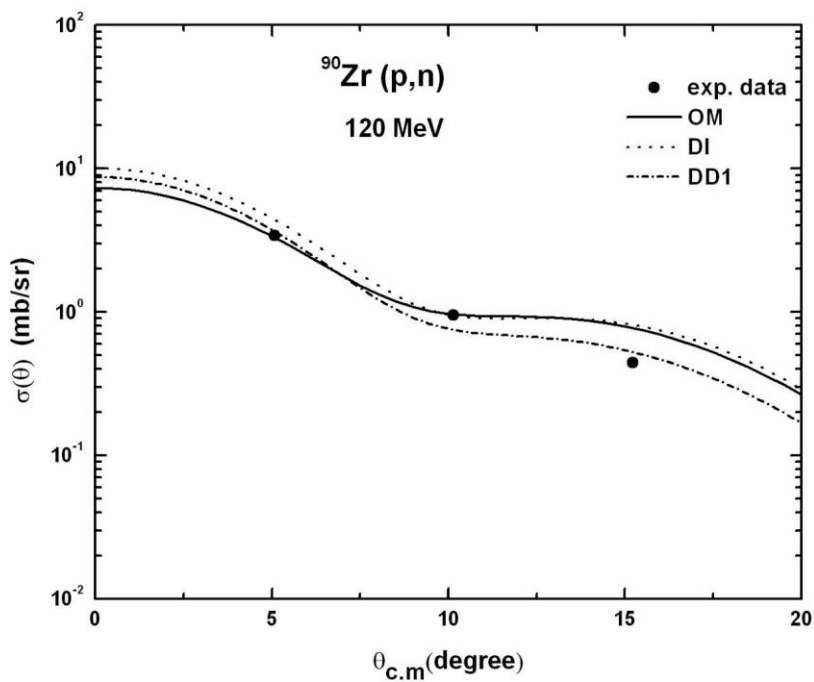
410

Fig. (3): Quasi-elastic scattering for ^{90}Zr (p,n) at 45 MeV.

411

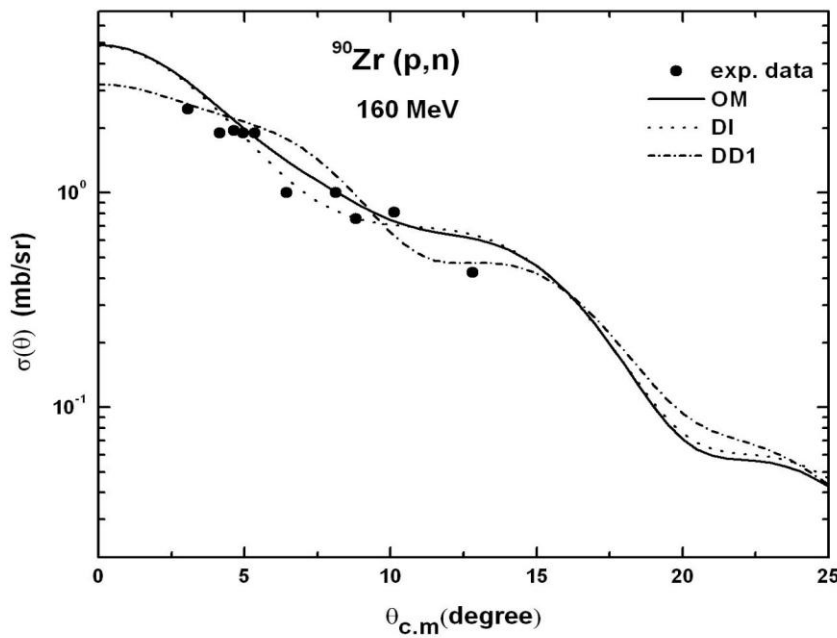
The data are taken from Ref.[10].

412



413
414 Fig. (4): Quasi-elastic scattering for ^{90}Zr (p,n) at 120 MeV.

415 The data are taken from Ref.[11].



416
417 Fig. (5): Quasi-elastic scattering for ^{90}Zr (p,n) at 160 MeV.

The data are taken from Ref.[12].

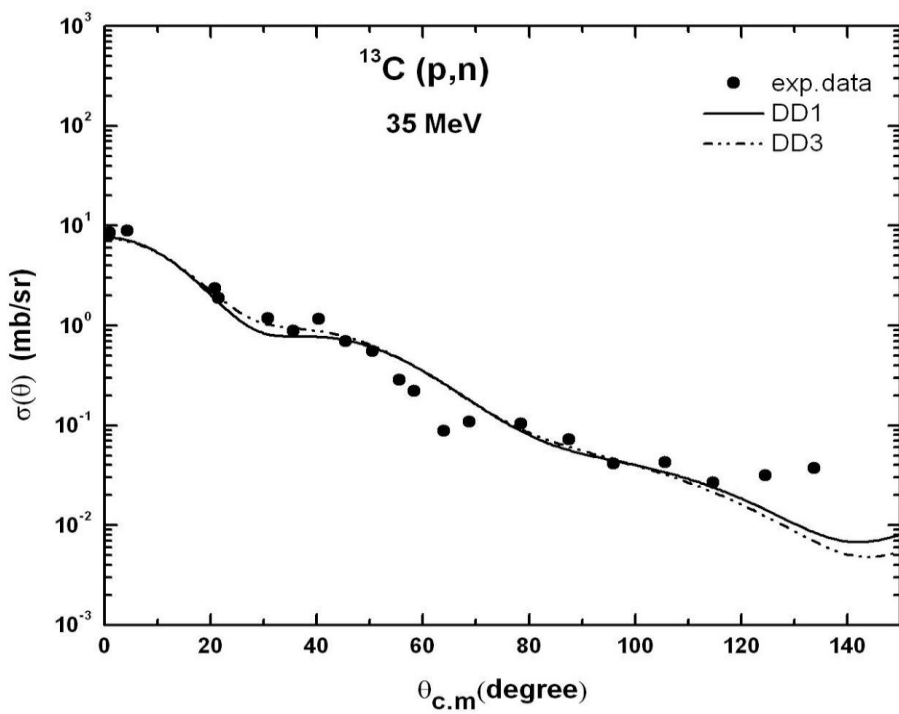
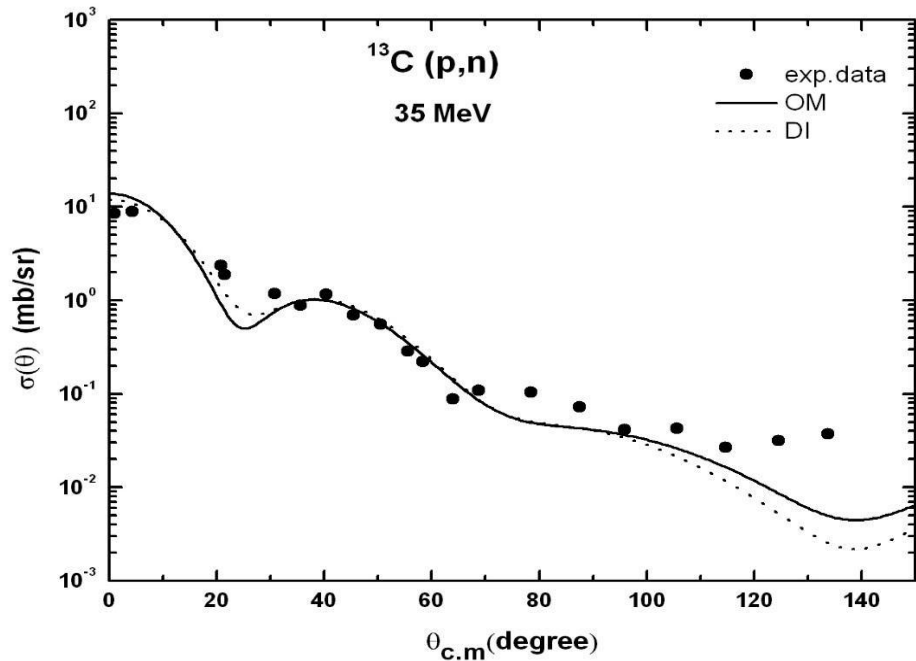
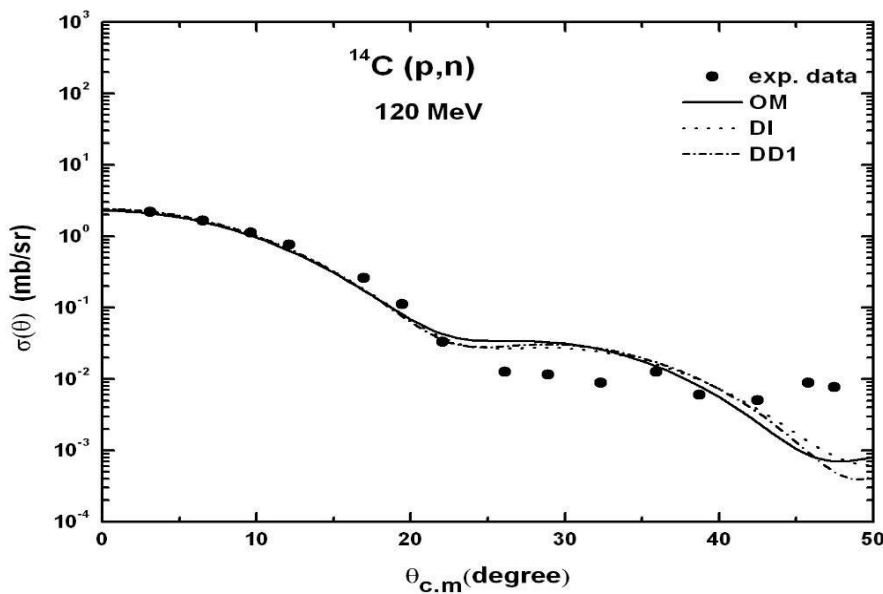


Fig (6): Quasi-elastic scattering for $^{13}\text{C}(\text{p},\text{n})$ at 35 MeV.

421 The data are taken from Ref.[[13,14].

422

423



424

425 Fig (7): Quasi-elastic scattering for $^{14}\text{C}(\text{p},\text{n})$ at 120 MeV.

426

The data are taken from Ref.[15].

427

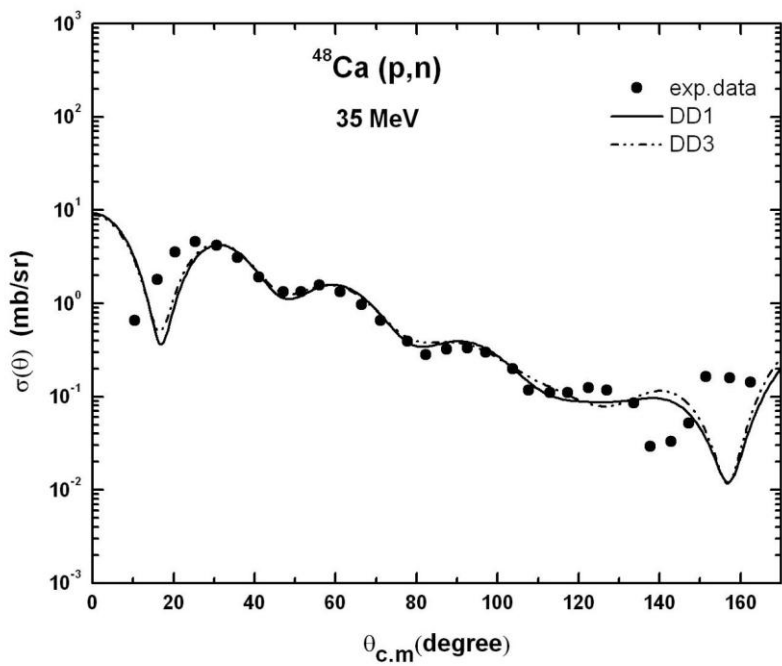
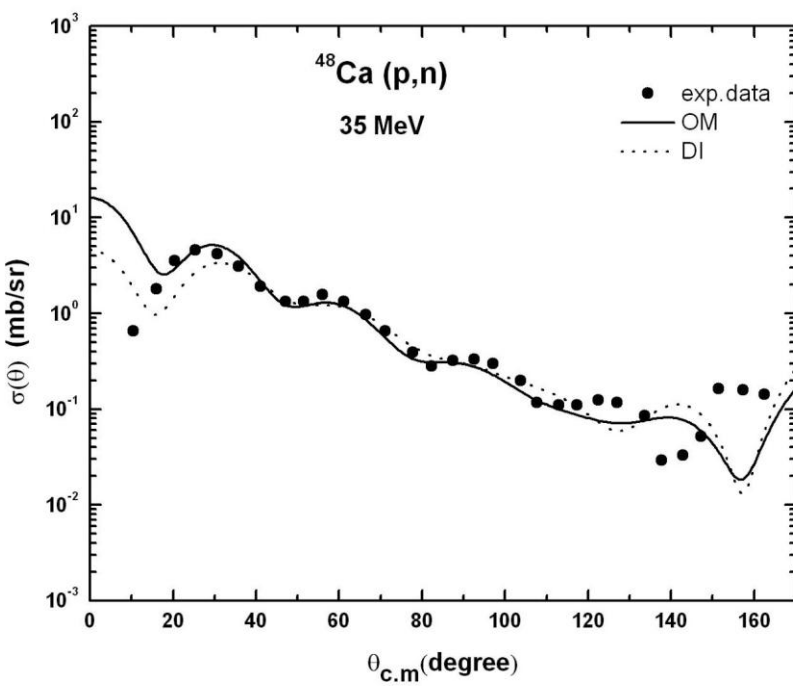
428

429

430

431

432



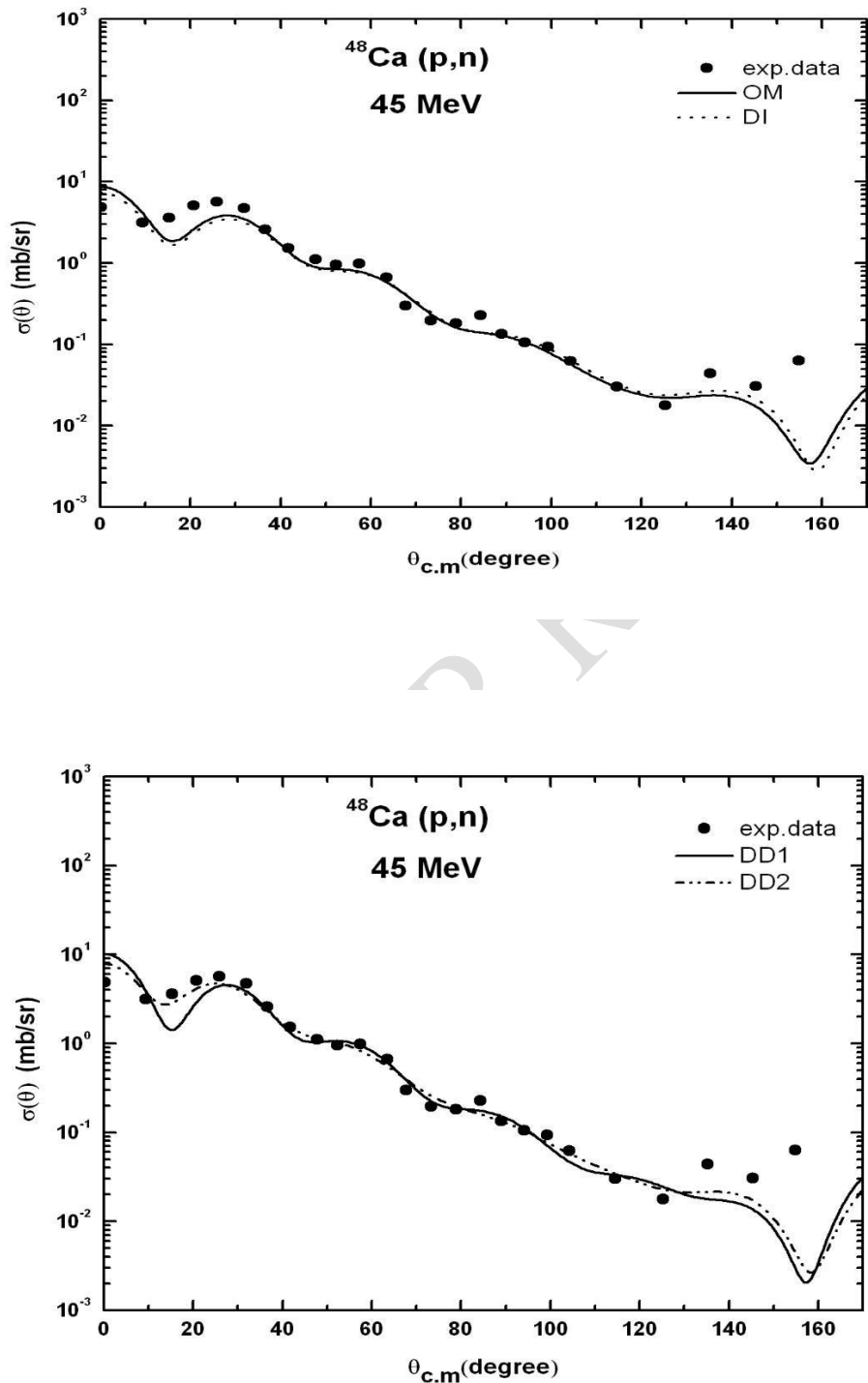
433

434

Fig. (8): Quasi-elastic scattering for ^{48}Ca (p,n) at 35 MeV.

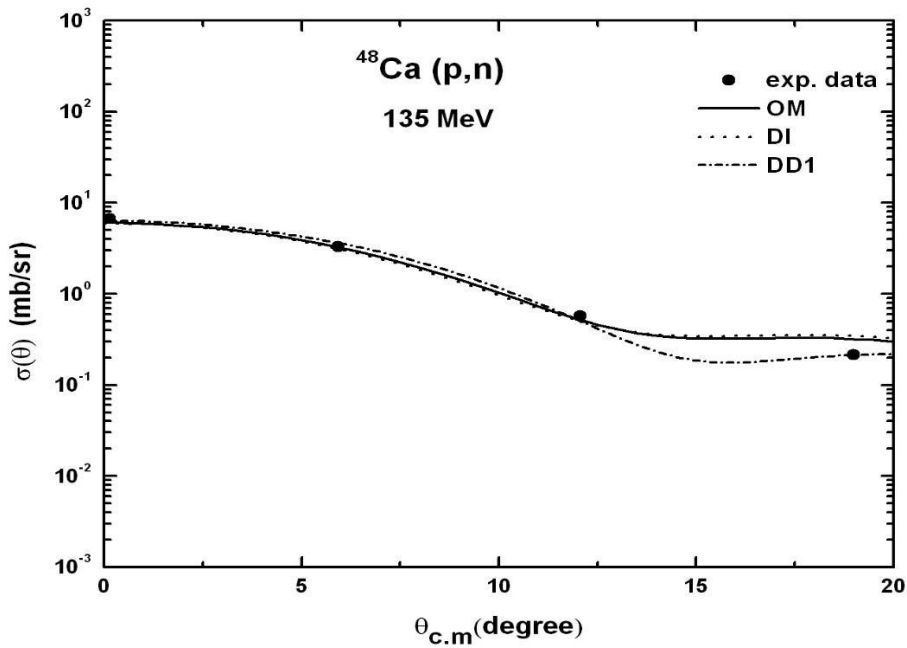
435

The data are taken from Ref.[10].

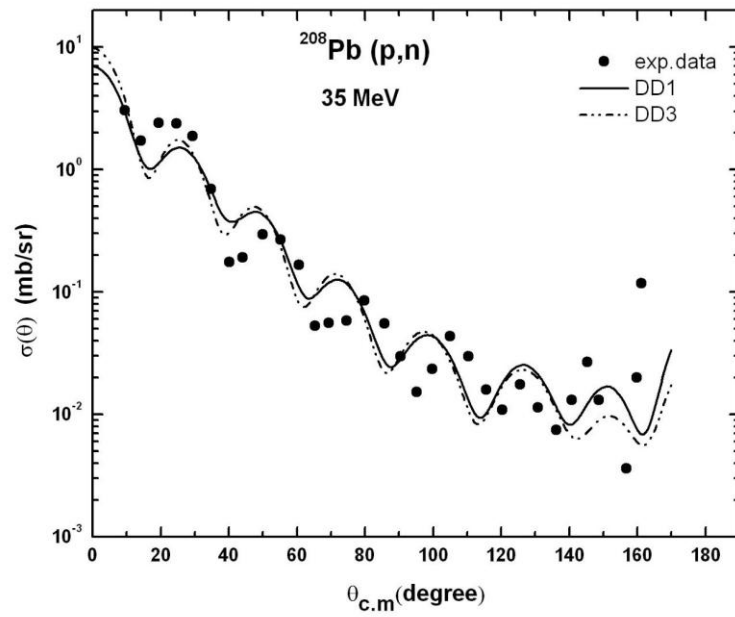
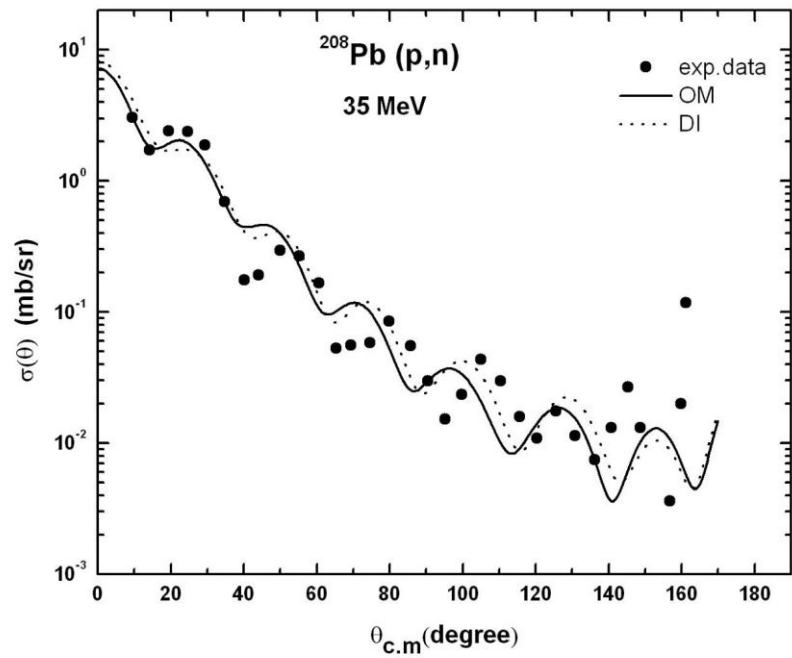
Fig. (9): Quasi-elastic scattering for $^{48}\text{Ca} (\text{p},\text{n})$ at 45 MeV.

The data are taken from Ref.[10].

440
441
442



443
444 Fig. (10): Quasi-elastic scattering for $^{48}\text{Ca} (\text{p},\text{n})$ at 135 MeV.
445 The data are taken from Ref.[16].
446
447
448
449
450
451
452
453
454
455
456
457
458
459
460

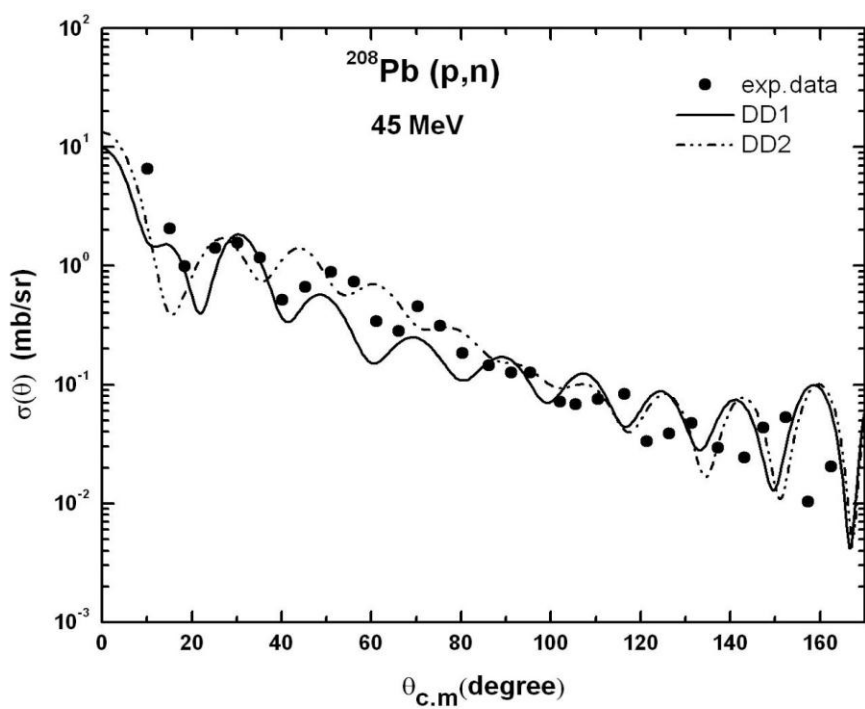
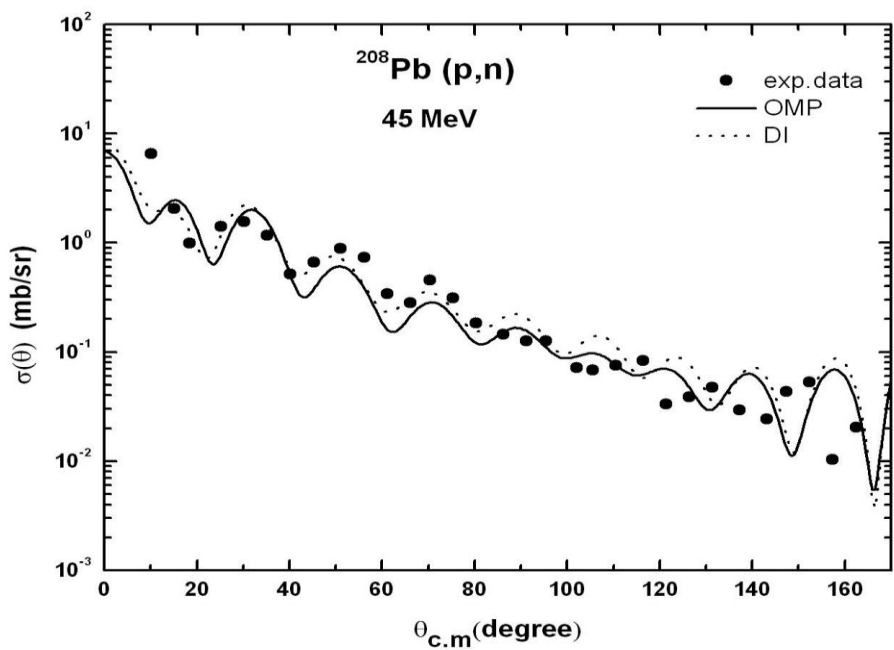


461

Fig (11): Quasi-elastic scattering for ^{208}Pb (p,n) at 35 MeV.

462

The data are taken from Ref.[10].



464

The data are taken from Ref.[10].

465

466

UNDER PEER REVIEW